

Vacuum formed coils for MRI

Karthik Gopalan¹ | Julian Maravilla | Jaren Mendelsohn | Ana C. Arias | Michael Lustig

Department of Electrical Engineering and Computer Sciences, University of California, Berkeley, California USA

Correspondence

Michael Lustig, Department of Electrical Engineering and Computer Sciences, University of California, Berkeley, CA 94720, USA.

Email: mikilustig@berkeley.edu

Funding information

GE Healthcare; National Institutes of Health, Grant/Award Numbers: R01MH127104, U01EB023829, U01EB025162, U01EB029427

Purpose: To describe a digital fabrication method used for custom MRI receive coils with vacuum forming and electroless copper plating.

Methods: Our process produces intricate copper traces on curved surfaces. A three-dimensional scan of a desired anatomy is obtained and used to design coil elements. The layout is predistorted with a self built simulation of the vacuum forming process and the geometric overlaps are tested with electromagnetic simulation software. The desired coil geometry is patterned onto a polycarbonate sheet by sandblasting through a tape mask. The sandblasted areas are then catalyzed with a palladium-tin solution and vacuum formed. The catalyzed, three-dimensional part is placed into a custom built plating tank and copper plated. Electronic components are attached to the copper traces to form resonant receive coils. The methods described here are demonstrated and tested with an 8 channel visual cortex coil array.

Results: The prototype coils exhibit quality factor ratios higher than three, indicating body noise dominance. The coil array shows high signal-to-noise ratio (SNR) near the periphery of a head shaped phantom. In vivo images with up to $0.37 \times 0.37 \times 0.67 \text{ mm}^3$ spatial resolution were acquired on a human volunteer.

Conclusion: This work presents the first example of vacuum formed coils with direct electroless copper plating. Our fabrication method results in coil arrays that are in close proximity to the body. This methods described here may enable the rapid development of a set of coils of different sizes for applications including longitudinal fMRI studies and MR-guided therapies.

KEYWORDS

coil, copper plating, MRI, RF, vacuum forming

1 | INTRODUCTION

MRI is a powerful and safe imaging modality that is widely used to visualize human anatomy. In order to acquire an image, MRI scanners use resonant radiofrequency (RF) receiver coils to detect a signal from excited nuclear spins. Arrays of these receivers are used to improve acquisition

times and increase the signal-to-noise ratio (SNR).¹ Traditionally, research in receive coils has focused on increasing channel counts. The individual coils are typically constructed with a loop of wire and ceramic capacitors attached to a rigid former.² Arrays designed with this method are time consuming to build and must be made to fit the majority of subjects. In the past several years, there

has been an effort to make coils that conform to the body in order to improve patient comfort and increase SNR. Numerous groups have shown that bringing coils closer to the subject improves image quality.³⁻⁵ Advances in additive manufacturing methods such as three-dimensional (3D) printing have enabled new innovations for coil design and form factor. For example, Zhang et al demonstrated a glove coil that couples a flexible mechanical design with a novel electronic circuit to capture high-resolution images of hands in motion.⁶ In addition, some groups have demonstrated new manufacturing techniques that should accelerate the coil fabrication process. For example, Corea et al developed a process for screen printing conductive inks onto a flexible Polyether Ether Ketone (PEEK) substrate to make MRI coils that conform to the subject.⁵ Though the coil arrays required manual tuning and assembly, the conductive traces and tuning capacitors were printed with a fast and reproducible process. Another novel method for creating receive coils was described by Vincent and Rispoli.⁷ The authors used a desktop sewing machine to create an MRI coil that could stretch in multiple directions by sewing conductive threads into stretchable athletic fabric. Despite a decrease in SNR compared to conventional coils, the stretchable coils could conform to almost any body part.

Many recent innovations in receive coil development have focused on flexible coils that can conform to the body. However, flexible coils cannot always conform to complex curved surfaces like the back of the head or neck. Our prior work patterning coil geometries on rigid 3D printed substrates showed that a form fitting coil improved central SNR by 1.4 \times and peripheral SNR by 5 \times compared to a commercially available alternative. The SNR was improved by bringing the coils as close as possible to highly curved anatomy.⁴ In addition, Keil et al. showed that placing a subject in a closely fitting head coil resulted in a slight improvement in central SNR and a 2 – 3 \times improvement in peripheral SNR.³ The authors developed five 32 channel receive coil arrays for different age groups using conventional coil construction methods. Their work showed the benefits of tailoring the coils to the body and choosing the correct coil size for the subject. However, conventional coil manufacturing methods are time consuming and require a skilled RF engineer. It is currently not practical or cost effective to have a wide range of coil sizes at every scanner site. In order to improve the speed of manufacturing, we developed a method to deposit coil traces on curved plastic substrates using a combination of vacuum forming, sandblasting, and electroless copper plating.

Vacuum forming is an industrial process where a plastic sheet is heated beyond its glass transition temperature and pulled over a mold. Once the plastic makes contact, a vacuum force is applied to force the sheet to conform to

the contours of the mold. We use vacuum forming to create MRI coil arrays that are in close proximity to specific body parts by making molds from digital MRI scans or 3D scans. To fabricate a coil array, we start with a plastic sheet that is prepared with a sandblasted pattern of the desired coil layout. Sandblasting uses air pressure to etch a surface by bombarding it with abrasive material like sand, glass beads, or metal particles. The patterned sheet is then sensitized with a palladium-tin catalyst and vacuum formed into the shape of a target anatomical structure. The formed plastic is copper plated, and electronic components like inductors, capacitors, and diodes are attached to make functional receive coils. To demonstrate our methods, we built and tested an eight-channel coil array to image the visual cortex. Since vacuum forming stretches a flat sheet into a 3D object it was not possible to uniformly pattern the coil layout. In order to account for the deformation inherent to vacuum forming, we designed a simulation of the vacuum forming process in C++. The simulation compensates for the distortion and stretching and generates a predistorted pattern that attempts to minimize areal distortion on the final 3D surface. We also developed a method to validate and correct the simulation by printing a grid on a plastic sheet, vacuum forming it to a known 3D model, and 3D scanning the grid. With our methods, it is possible to make dense three dimensional conductor designs and pattern traces over complex curved surfaces.

2 | METHODS

The process flow for creating a vacuum formed MRI receive coil array starts with a 3D scan of a specific body part. The 3D scan can be created with a 3D scanning device such as the Structure Sensor (Occipital) or from a 3D MR scan combined with 3D segmentation software such as Horos (Horos Project, <https://horosproject.org>). The scan is used to prepare a layout of coil geometries with custom built vacuum forming simulation software. Next, the 3D model is turned into a mold by CNC milling a negative of the model out of foam and filling the negative with gypsum cement. A flat plastic sheet is then covered in a tape mask and the predistorted coil geometries are cut out with a laser cutter (Figure 1A). Next, the exposed areas of the plastic are sandblasted, cleaned, and catalyzed for copper plating (Figure 1B,C). The mask is removed and the flat plastic sheet is vacuum formed into the shape of the mold (Figure 1D). After vacuum forming, the 3D plastic substrate is removed from the mold and placed into a copper plating tank (Figure 1E). The copper traces are then tin plated to make them more stable in open air. Electronic components are used to connect the traces and form functional MRI receive coils.

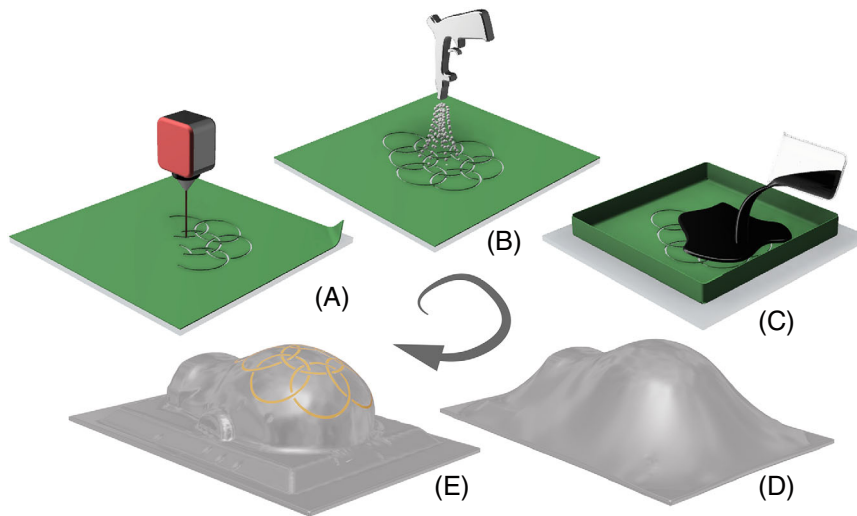


FIGURE 1 (A) A polycarbonate sheet is masked with polyester tape and the pre distorted coil pattern is cut out of the mask with a CO₂ laser. (B) The sheet is sandblasted with 100 grit white fused aluminum oxide. (C) After cleaning, the exposed areas are catalyzed with a palladium-tin solution. (D) The mask is removed, and the sheet is vacuum formed. (E) The vacuum formed plastic is removed from the mold and copper plated in an aqueous solution of copper sulfate, ethylenediaminetetraacetic acid, sodium hydroxide, and formaldehyde.

2.1 | Vacuum forming simulation

In order to predict the deformation inherent to vacuum forming, we developed a graphical simulation in C++ using OpenGL. Our simulation models the plastic as a discrete network of point masses and springs. The point masses are connected with edges in order to triangulate the surface. Collisions for arbitrary objects, including the build platform and mold, are handled with the Embree ray tracing kernel.⁸ The initial state of the simulation is shown in Figure 2A. The figure shows a digital plastic sheet raised over a mold to be vacuum formed. The modeled plastic sheet is lowered over a 3D model as shown in Figure 2B. We assume that the plastic experiences infinite friction when it collides with the mold⁹ and will stick to the surface. In Figure 2C, the sheet makes contact with the base of the vacuum former and vacuum is applied to force the plastic to conform to the mold. Figure 2D shows the final state of the simulation when the entire sheet has made contact with the mold or the platform. The vacuum force (F_{vac}) is modeled as a force proportional to the area (A) of each triangle and a user defined constant p applied along the normal (\hat{n}) vector of the triangle, as shown in Equation (1).

$$F_{\text{vac}} = -pA\hat{n}. \quad (1)$$

We also integrated portions of the computational geometry algorithms library to perform an as rigid as possible planar parameterization of the deformed plastic sheet.^{10,11} The parameterization allows the user to provide a two-dimensional image of an undistorted design and get a pre-distorted image that attempts to minimize areal distortion when applied to the 3D model. An example of a distorted pattern created with this method is shown in Figure 2E,F. The figures show that uniformly patterned

coil geometry stretches undesirably after vacuum forming while the pre-distorted pattern creates more reasonable loops on the 3D model.

2.2 | Verification of vacuum forming simulation

In order to verify the deformation simulation, we printed a grid on a polycarbonate sheet with a Sharpie marker attached to our CNC milling machine (Figure 3A). Before drawing the grid, the sheet was sandblasted in order to provide a nonreflective surface. Reflections from the plastic interfere with the photogrammetry software and introduce errors in the 3D reconstruction. The gridded sheet was then vacuum formed to a head-shaped mold and the formed plastic was imaged with a cell phone camera from multiple angles. An example image is shown in Figure 3B. The images were uploaded to a cloud-based photogrammetry software called Recap (Autodesk) to generate a digital 3D model (Figure 3C). The texture map is then extracted from the 3D model and displayed with Cairo, a two-dimensional graphics library (Figure 3D). A low pass filter is applied to the texture and the grid is reconstructed by labeling the contours of the deformed white squares with OpenCV. The labeling is shown in Figure 3E. The centroids of the labeled boundaries are connected to form a mesh which corresponds to the final position of the uniformly patterned grid after vacuum forming (Figure 3F). This connected mesh is uniformly scaled, rotated, and translated to be as close as possible to the simulated mesh by minimizing the euclidean distance between simulated and experimentally measured points. Grid points that were obscured by noise were ignored.

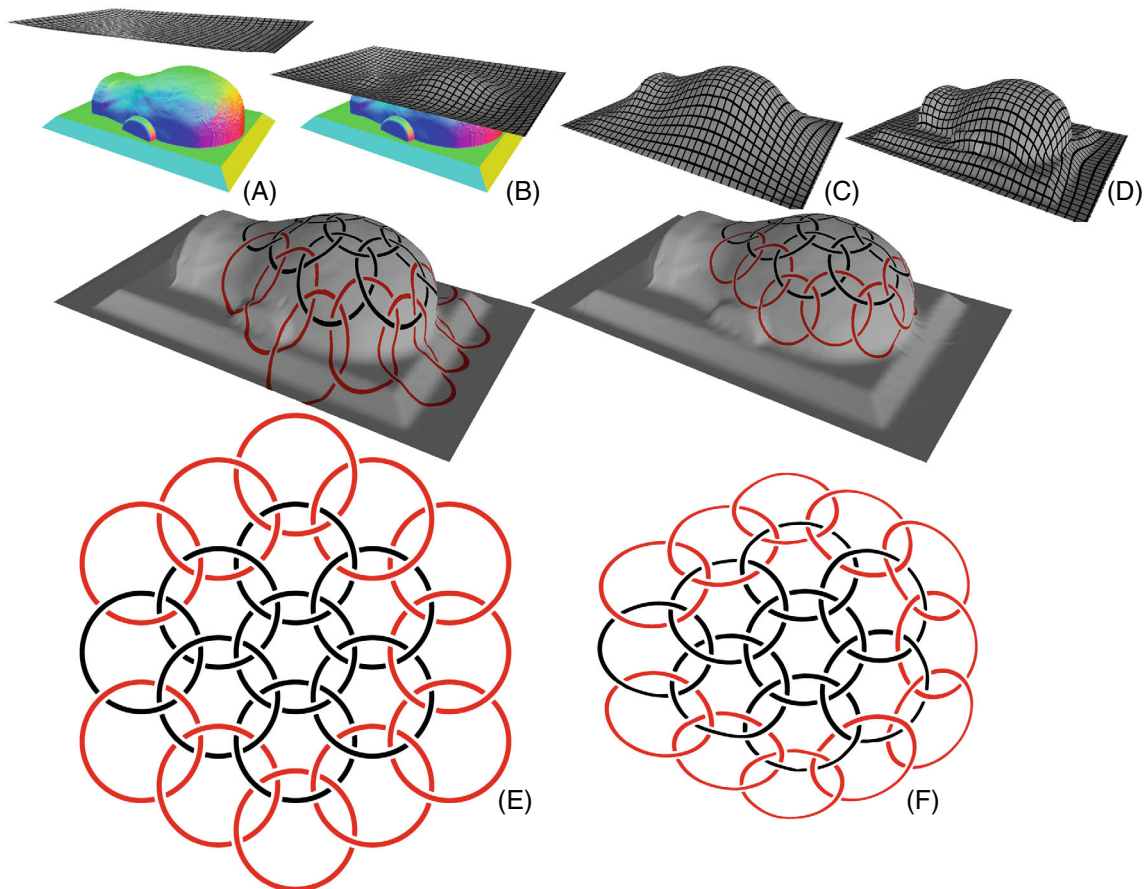


FIGURE 2 Example of the vacuum forming simulation with a head model. (A) The initial state of the simulation. (B) The plastic sheet starts to intersect the model. (C) The sheet then intersects the base before a vacuum force is applied. (D) The final state of the simulation after the vacuum force is applied and all points of the sheet are stuck to the model. (E) The two-dimensional undistorted coil array design and the result of naively applying it before vacuum forming. Out of the 19 elements shown, the eight black channels were used for our prototype coil array. (F) The predisformed design created with an as rigid as possible planar parameterization produces coils with less deformation.

2.3 | Electromagnetic simulation

In addition to the mechanical simulation, electromagnetic simulations were used to determine the electrical performance of the vacuum formed coils. Closely placed MRI receiver coils couple inductively increasing the complexity of tuning and matching. This effect can be mitigated by adjusting the overlap between neighboring coils in order to minimize the mutual inductance. To determine the critical overlap on a complex vacuum formed surface, the aid of an electromagnetic simulation software (HFSS, Ansys Inc.) in combination with electronic design automation software (ADS, Keysight Technologies) was used to optimize coil placement.

A Tri-Coil layout (Figure 4A) was used to model the eight-channel coil pattern used for the head array. This layout provides enough information to determine the overlap need between elements for a larger scale array. The Tri-Coil pattern was wrapped on a curved surface to mimic the shape of the back of a head (Figure 4B). Coil placement

is determined by the distance between centers of neighboring coils (d) and the diameter of an individual coil (D). Multiple simulations were executed by varying the distance between coils until the mutual inductance was minimized. When d/D is near $3/4$'s, the coupling between the elements was minimized (Figure 4C,D). The optimal overlap varies depending on the exact curvature of the surface. However, for mild curvature the optimal point is still near $3/4$'s which means that coil overlap can be set to $3/4$'s without much degradation to geometric decoupling performance. Nevertheless, this simulation can be applied to many curvilinear surfaces and be used to characterize the geometric decoupling performance of different vacuum formed coils.

2.4 | Mold preparation

Mold standard tessellation language (STL) files are prepared from 3D MR scans using surface reconstruction tools

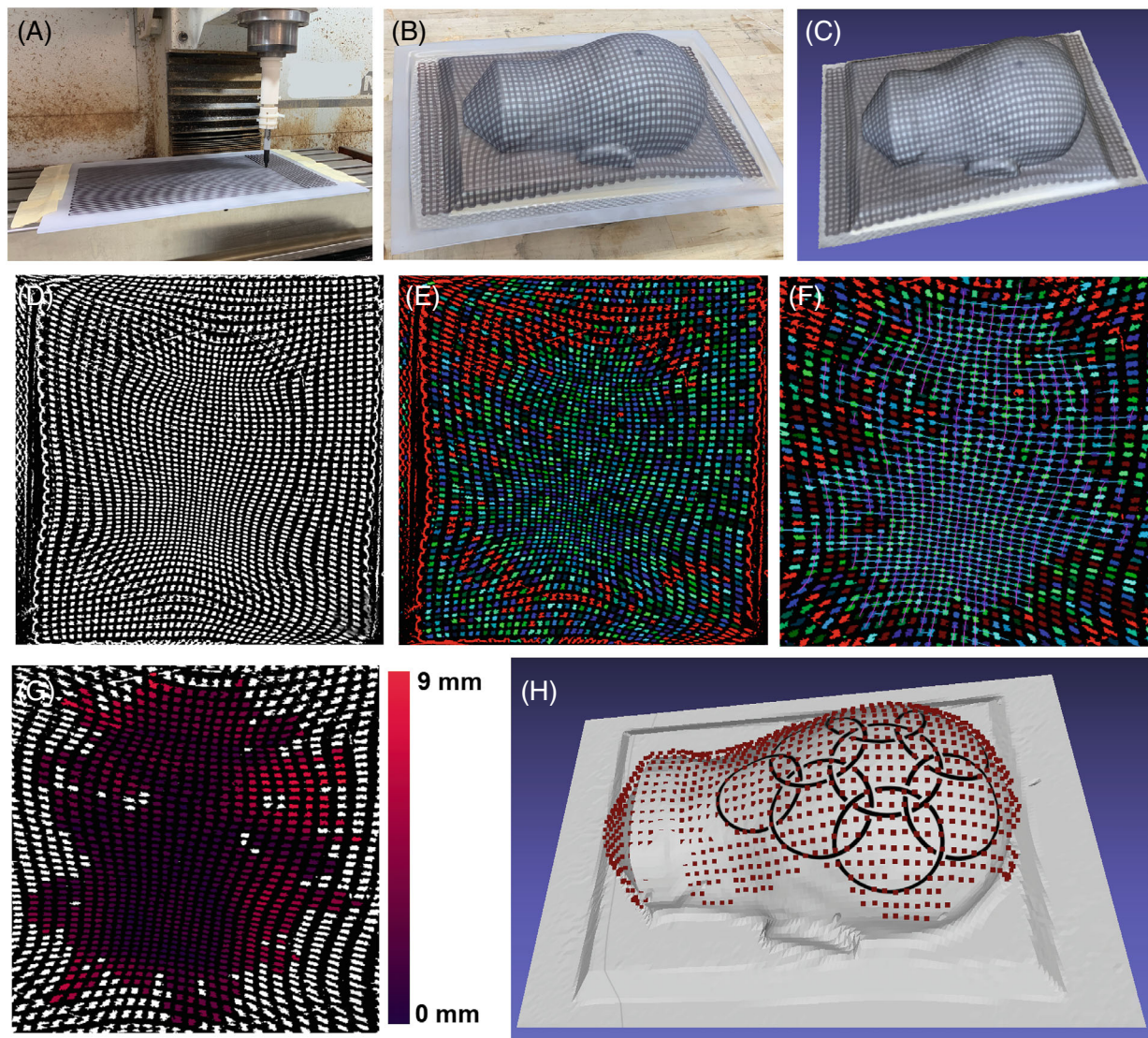


FIGURE 3 Verification of vacuum forming simulation. (A) Printing a grid on a flat polycarbonate sheet with our CNC milling machine. (B) A single image of the vacuum formed plastic to be used for photogrammetry. (C) Reconstructed three-dimensional (3D) model of the vacuum formed plastic with grid lines. (D) Flattened model texture. (E) Texture with labeled contours. Red indicates shapes which are filtered out due to being nonrectangular, and the remaining rectangles are colored a random mixture of blue and green to distinguish them from each other. (F) Re-forming the grid from adjacent rectangles, blue/purple lines indicate correct grid lines. (G) Relative error of squares where connectivity succeeded, darker purple indicates lower error while brighter red indicates higher error. The dimensions of the plastic substrate are 280 mm × 432 mm. The maximum percentage error with respect to the length is 2%. Error was not calculated for the white squares due to the noise of the scan. (H) 3D reconstruction of scanned grid points shown in red and overlaid on a simulated model of a vacuum formed sheet.

in Horos (Horos Project, <https://horosproject.org>). These files are edited with Meshmixer (Autodesk) in order to remove internal geometry like the brain and skull. The visible faces are first selected with a brush tool and the selection set is inverted to delete the unwanted parts of the model. The remaining surface is smoothed with the RobustSmooth brush to reduce the layering artifacts from the surface reconstruction. An example of a finished head model is shown in Figure 5A. Next, a machining toolpath is designed with Fusion 360 (Autodesk) and the negative of the digital models are cut out of laminated insulating

foam (Foamular 150, Owens Corning) with a Tormach 1100M milling machine (Figure 5B). We used a six inch long, quarter inch diameter carbide ball end mill. The foam block is made by laminating sheets with a thin layer of Gorilla Glue and clamping overnight. After milling, we pour Perfect Cast casting material into the negative along with two bolts and a brass tube running to the top of the mold for blowing compressed air after vacuum forming (Figure 5C). The bolts are used to mount the gypsum mold to a wooden support. We also experimented with making positive molds out of wood and aluminum but

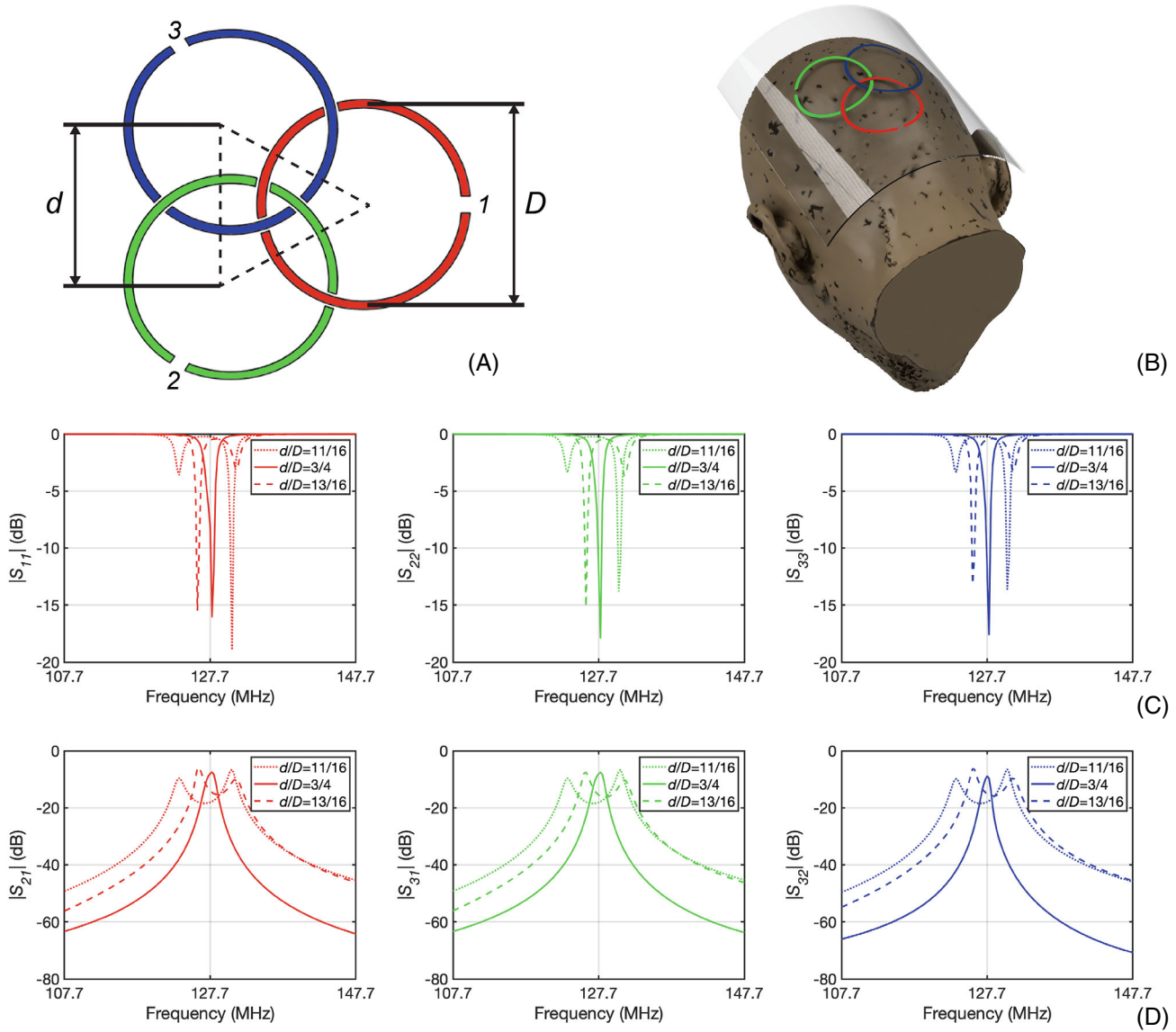


FIGURE 4 Geometric decoupling simulation. (A) Tri-Coil pattern used in HFSS/ADS simulation. The ratio of the distance between the coils and the diameter of the coils was used to classify the overlap between the elements. Excitations were assigned to ports 1, 2, and 3 in HFSS. Those results were placed into ADS for tuning and matching. (B) Three-dimensional model of Tri-Coil pattern on a curvilinear surface. This surface was used to mimic the back of the head. (C) Return loss for each coil. The optimal return loss is achieved when the ratio of overlap to diameter is approximately 3/4's. (D) Coupling between the coils for each pair. When the overlap to diameter ratio is approximately 3/4's the coupling between the coils is minimized and no resonant splitting occurs.

the gypsum and foam were more cost effective for larger models.

2.5 | Substrate preparation

A polycarbonate sheet (TAP Plastics) is dried overnight in an oven set to 110°C to prevent absorbed moisture from creating bubbles and surface imperfections during the vacuum forming process. Two layers of 90 μm (3.5 mil) polyester powder coating masking tape (Advanced Polymer Tape) are applied to the plastic sheet with a rubber

roller. A pattern is then cut out of the tape with a CO₂ laser (Universal Laser Systems). Next, the exposed areas of the plastic are sandblasted with 100 grit white fused aluminum oxide blasting media (Industrial Supply). Sandblasting is used to increase the surface area of the plastic and is essential for copper adhesion. The substrate is then cleaned with deionized water and Alconox cleaner. The substrate is then treated with a 1% aqueous solution of benzalkonium chloride which is a cationic surfactant used to improve the adhesion of the catalyst. After rinsing, the edges of the tape are peeled upward to make a small reservoir around the laser cut mask. This method is used to reduce the amount

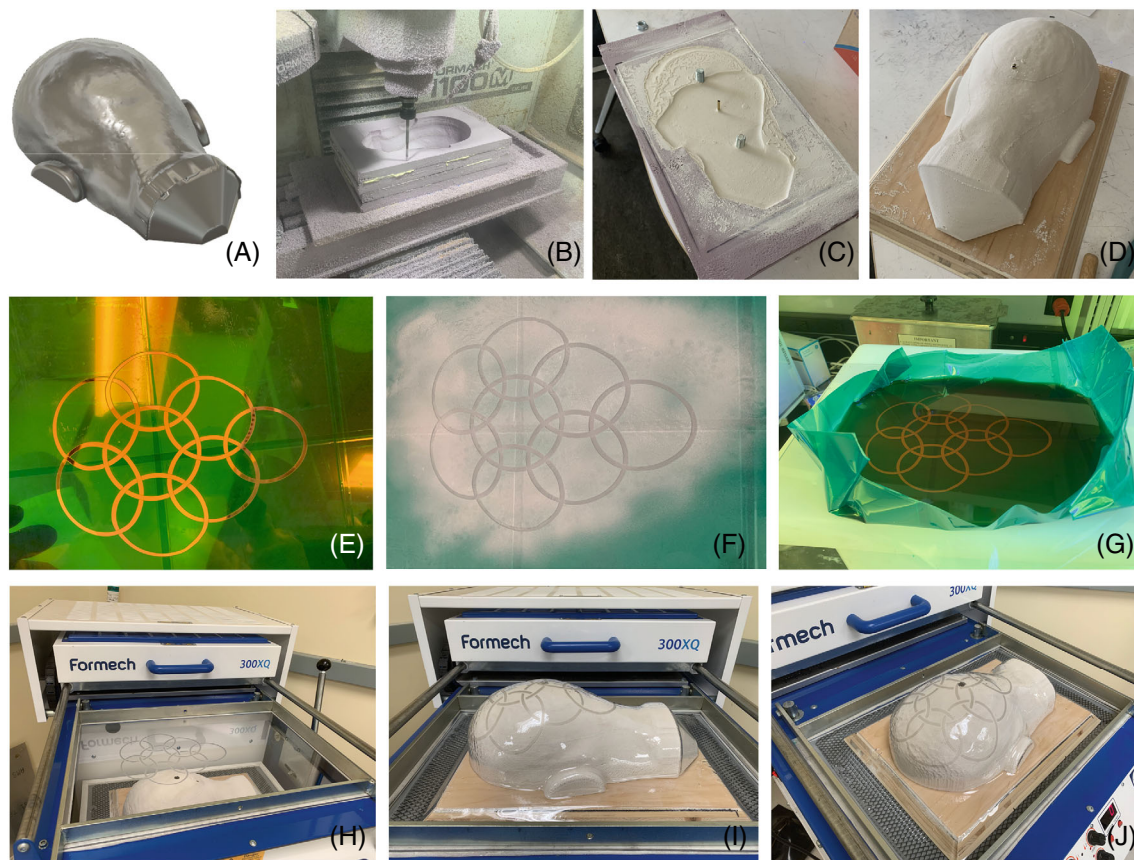


FIGURE 5 The physical process steps of creating our 8 channel visual cortex coil. (A) A digital model of the back of a subjects head is created from three-dimensional MRI scan data. (B) The negative of the head mold is milled out of insulating foam with a CNC milling machine. (C) Casting plaster is cast into the foam. (D) The foam is removed and the cast mold is attached to a wooden support. (E) A predistorted coil layout is laser cut out of a tape mask. (F) The design is sandblasted into a polycarbonate sheet. (G) After cleaning, a catalyst is poured into a well made out of the tape. (H,I,J) The tape mask is removed and the catalyzed plastic is vacuum formed over the head shaped mold.

of copper plating catalyst solution required. The catalyst is prepared by adding 60 ml of 37% hydrochloric acid and 0.25 g palladium chloride (PdCl_2) to 1 L of deionized water. 12 g of tin chloride (SnCl_2) is added when the palladium salt completely dissolves and the solution is ready after one hour of stirring at 40–50°C.¹² The catalyst can be prepared and stored until the salts crash out of solution. The catalyst is then poured into the tape reservoir and allowed to sit for 10 min.

2.6 | Vacuum forming

After catalyzing, the substrate is rinsed in deionized water and the tape mask is removed. The polycarbonate is vacuum formed over a mold of the desired geometry with a Formech 300XQ vacuum former. The vacuum forming machine has five heating zones consisting of a large element in the center and four elements on the edges. We found that setting the central element to 70% and the others to the maximum reduced vacuum forming artifacts

such as wrinkles and folds near the corners of the mold. The substrate is heated for approximately 120 s until it drooped uniformly in the center. Next, the mold is raised into the soft substrate and a vacuum is pulled simultaneously until the substrate makes complete contact with the mold.

2.7 | Electroless plating

After vacuum forming, the mold is removed and the edges of the plastic are cut with a bandsaw to prepare for copper plating. The copper plating solution is prepared with 18 g/L copper sulfate pentahydrate ($\text{CuSO}_4 \cdot 5\text{H}_2\text{O}$), 48 g/L ethylenediaminetetraacetic acid, 57.3 mg/L potassium ferrocyanide ($\text{K}_4[\text{Fe}(\text{CN})_6]$), and 1 ml/L concentrated 37% hydrochloric acid.¹³ The ethylenediaminetetraacetic acid is a complexing agent that binds with the copper ions to make them more soluble in water. The potassium ferrocyanide is a safe chemical that brightens the copper deposits by promoting a smaller copper grain size and

slightly reducing the plating rate.¹⁴ The hydrochloric acid is used to increase the amount of chloride ions in the solution which modulates the plating rate. Sodium hydroxide (NaOH) is used to raise the pH to 12.8 and 22.5 ml/L of 37% formaldehyde is added as a reducing agent just before plating. We also built a plating tank (Figure S1A) including a 14-L polypropylene tank, a plastic circulation pump, a 25 micron filter bag, and a plywood support structure. The vacuum formed part is submerged in the plating tank with vigorous nitrogen bubbling. The nitrogen displaces the dissolved oxygen in the bath to prevent the formation of copper oxides. In addition, the agitation from the bubbling helps dislodge hydrogen gas bubbles created from the plating reaction. The plating is performed at room temperature. We measured a plating rate of 5 μm per hour by plating on a smooth polycarbonate sheet, removing the copper, and measuring the film thickness with a Mitutoyo 293-340-30 micrometer with an accuracy of 1 micron. Since RF currents run on the surface of conductors, we limited the plating time to 5 h for our coils that operate at 127 MHz. An example of a plated sample is shown in Figure S1B. Using our technique, we are able to pattern conductors on complex 3D surfaces. Soldering is also possible (Figure S1C) if care is taken not to melt the polycarbonate. We also use an immersion tin plating solution to passivate the surface of the copper. The aqueous solution is composed of 4 g/L tin chloride (SnCl_2), 50 g/L thiourea, and 12 ml/L sulfuric acid (H_2SO_4). The solution is heated to 90°C and the copper traces are submerged for approximately 30 s to coat them in tin.

2.8 | Coil tuning and matching

After the copper traces are patterned on the substrate, the gaps between the traces are connected with flexible PCBs (PCBWay) that have pads for soldering rigid tuning capacitors. We then solder another flexible board that contains matching and q-spoiling circuitry to each channel. The coil elements are completed by attaching electronic components according to the circuit diagram in Figure S2A. This topology uses a tuning capacitor for q-spoiling since the lower capacitance provides a higher blocking impedance. We use 1111 nonmagnetic capacitors (Passive Plus), ceramic chip inductors (Coilcraft), and nonmagnetic RF PIN diodes (Macom MA4P7470F-1072T). The loop is first tuned by measuring with a lightly coupled double probe and adjusting the tuning capacitors C_t until the resonance is close to 127.7 MHz. Next, the coil is connected directly to the network analyzer through a half wavelength RG316 cable and the matching capacitor C_m is adjusted to match the impedance to 50 Ω (Figure S2B). The coil is then connected to a 16-channel preamplifier

box (Clinical MR Solutions) and the output of one channel is connected to one port of the network analyzer. The coil is then probed with a pickup loop connected to the other port of the network analyzer. The measurement setup is illustrated in Figure S2A. L_{pre} is adjusted to resonate with C_m and the cable length is reduced until the observed dip from preamplifier decoupling is centered around the Larmor frequency as shown in Figure S2C. A bias-T is used to protect the analyzer and apply a 5-V DC signal to turn on the PIN diode through the output of the preamplifier. Finally, the inductor L_Q is adjusted until the received signal is in the noise floor at the desired resonant frequency as shown by the red trace in Figure S2C.

Subsequent elements are tuned independently by detuning all of the other channels with the PIN diodes turned on or one tuning capacitor removed.

2.9 | Cable traps

We designed and built inline traps to suppress common mode currents on the shields of the coaxial cables. The inline traps are made by winding the coax around a PCB former as shown in Figure S3A,B. The shield is then exposed on both sides of the winding by removing the jacket with a curved scalpel blade. The exposed shields are soldered to pads on the PCB and a capacitor is soldered across the winding to form a resonant circuit (Figure S3C). The traps are shielded by wrapping a 3D printed shell with copper tape (Figure S3D). These parts are made with clear resin with a Formlabs Form 2 3D printer. The devices with the shields are tuned to 127.7 MHz over a large ground plane with an Agilent Technologies E5061A network analyzer (Figure S3E). Insertion loss of at least 20 dB was reported for each of the traps at 127.7 MHz (Figure S3F). The tuned traps are attached approximately 8 cm away from the Q-spoiling circuitry of each channel.

2.10 | Phantom imaging

Coil testing was performed with a head-shaped loading phantom. The phantom was constructed with two polycarbonate sheets vacuum formed into the shape of the back of a head. The two halves were joined together with nylon screws and a laser cut silicone gasket. The phantom was filled with a solution made with deionized water, 2.4 g/L NaCl, 3.37 g/L $\text{NiCl}_2 \cdot 6\text{H}_2\text{O}$. The additives are used to increase conductivity and shorten T1 recovery and T2 relaxation times. SNR measurements for our eight-channel visual cortex coil were performed on a Discovery 3T MR750W scanner (GE Healthcare). The two-dimensional gradient echo scans had a repetition time

of 2000 ms, an echo time of 10 ms, a voxel size of $1.2 \times 1.2 \times 5 \text{ mm}^3$, a bandwidth of 122 Hz/pixel, and 16 slices. Data were collected in the sagittal, coronal, and axial planes. Noise measurements were acquired with the same imaging parameters but with the RF transmit coil turned off. SNR maps were calculated in absolute units using noise prewhitening and optimal coil combination following the methods of Kellman et al.¹⁵

To verify coil detuning, B1 maps were acquired with a GE product B1 mapping sequence. The sequence was run with the coil in place and repeated after carefully removing the coil without changing the position of the phantom.

Following B1 mapping, the coil was heat tested according to the scanner manufacturer's protocol. This consists of placing the coil array in the scanner without a phantom. The transmit gain is increased and the gradients are turned off. The heat testing sequence is a two-dimensional GRE with a echo time of 7 ms, repetition time of 18 ms, and a 90° flip angle. The specific absorption rate monitor is disabled and the scan is run for 15 minutes. The coil array, traps, and preamplifier box are imaged with a FLIR E4 thermal camera (Teledyne FLIR) to detect hot spots. Next the scan is repeated for 1.5 h with thermal probes placed around the custom hardware.

2.11 | In vivo imaging

After obtaining informed consent, a subject was placed in the coil array and scanned. The scan was performed at UC Berkeley under an Institutional Review Board (IRB) approved protocol (2013-07-5491). Images were acquired with a GE built in 3D T₁-weighted Bravo sequence. The scan is an inversion recovery prepped, fast spoiled gradient echo (FSPGR) sequence. Images were taken with varying resolution.

3 | RESULTS

3.1 | Verification of vacuum forming simulation

We are able to quantify the total error in the simulation as the sum of the euclidean distances between each simulated grid point and its equivalent real-world point (Figure 3H). Given this error, we ran a sweep of adjustable parameters in the simulation. Since the vacuum formed plastic is modeled as a set of point masses coupled with springs, these parameters include the spring constants, damping factor, density, and mass. These values were swept to find a set that minimized the global error between the output of the simulation and the reconstructed grid from the

TABLE 1 Average surface roughness of sandblasted and manually sanded polycarbonate

Sandblasting pressure (psi)	R _a (nm)	Sandpaper grit	R _a (nm)
50	1370.49	120	1632.41
75	2193.37	320	704.53
100	2754	Bare	19.96

3D scanned vacuum formed plastic. Each parameter was optimized individually while holding the others fixed. We found the per-point average error between the simulation and scanned model to be 2.8 mm with nonideal parameters and 2.5 mm with the optimal parameters (Table 1).

3.2 | Characterization of surface roughness and copper plating

The surface preparation before plating was optimized by copper plating small strips of polycarbonate with various surface treatments. Our initial experiments shown in Figure S4 consisted of manually sanding polycarbonate samples, copper plating them, and conducting a tape test to analyze copper adhesion. As illustrated by the figure, copper adhesion on bare polycarbonate is quite poor so a surface treatment is required. Adhesion tends to improve with increased surface roughness. Regions with an average surface roughness (R_a) of greater than 2 μm consistently passed tape and scratch tests after copper plating. The surface roughness of the polycarbonate samples was measured with a profilometer (Veeco Dektak 6M Stylus Profilometer). Compared to manual sanding, sandblasting provided a more uniform and repeatable surface roughness. With manual sanding, it was also not possible to sand close to the edges of the tape mask.

3.3 | Eight-channel visual cortex coil

The methods described above were used to design and build an eight-channel coil array for imaging the visual cortex. All of the physical process steps are illustrated in Figures 5 and 6. A digital 3D model of the back of a head was derived from MRI scan data. The model was modified to accommodate the subject's ears and the ends were tapered to help with the removal of the plastic after vacuum forming. We then fabricated a vacuum forming mold by casting plaster into a CNC milled negative of the head model. A predistorted pattern of an eight-channel coil design was created with the aid of our vacuum forming simulation software. That pattern was laser cut out

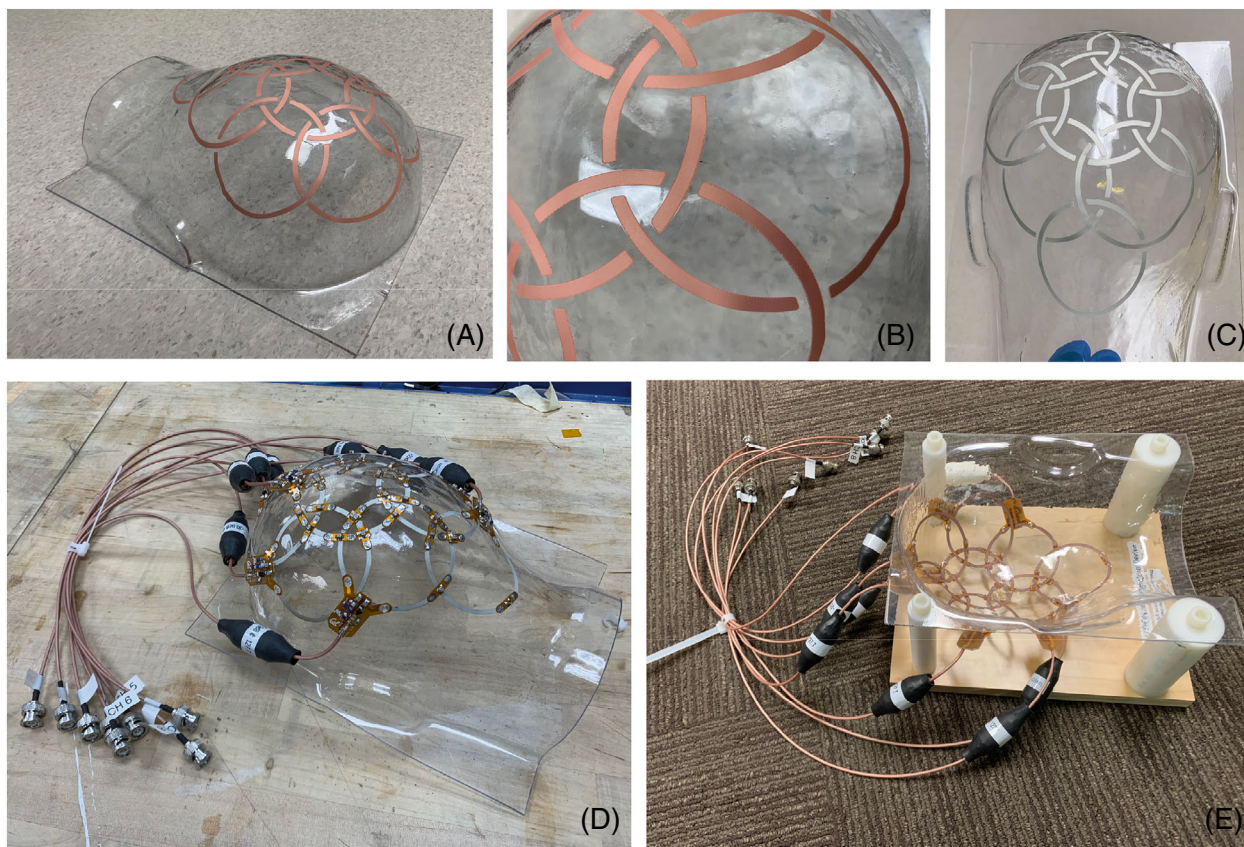


FIGURE 6 Copper plating and populating the vacuum formed substrate. (A) The mold is removed, the plastic is trimmed with a bandsaw and the traces are copper plated. (B) A close up of the copper reveals a high quality surface finish. (C) The copper is passivated with an immersion tin solution. (D) Rigid components including cables, traps, and tuning capacitors are added to properly tune and match the coil array. (E) The coil is attached to a support created with delrin rods, nylon screws, and plywood.

of a tape mask and sandblasted into a polycarbonate sheet as shown in Figure 5E,F. The tape mask was used as a container for a cleaning solution, a surfactant, and a palladium-tin catalyst which was used to prepare the sanded surfaces for copper plating (Figure 5G). The tape was removed and the catalyzed plastic sheet was vacuum formed over the head-shaped mold (Figure 5H,I,J). The plastic was removed from the mold, trimmed with a bandsaw, and placed into our custom made plating tank (Figure S1A). After removal from the plating tank, the substrate was rinsed and the copper traces were submerged in an immersion tin plating solution (Figure 6A–C). All coils were then tuned and matched with discrete components and flexible printed circuit boards. The final coil array is shown in Figure 6D,E.

The individual channels of our coil had an average unloaded Q of 146 and an average loaded Q of 29. The Q -ratio of our coils was 5.03 which indicated body noise dominance. A copper tape coil constructed with the same flexible circuit boards on a polycarbonate substrate produced an unloaded quality factor of 175. Network analyzer measurements revealed a strong match with a return loss

of more than 30 dB per channel when placed on a loading phantom. This is shown in the S11 plot in Figure S2B. The Q spoiling circuitry detuned the coils by 63 dB and brought the frequency response to the noise floor at the Larmor frequency (Figure S2C).

The SNR maps (Figure 7A,B) revealed high peripheral SNR with the highest signal exhibited near the surface of the coils. This is due to the coil proximity which is intrinsic to the vacuum formed coil manufacturing method. Since the plastic conforms to a mold of the desired anatomical features, the coils are as close to the subject as possible while maintaining a safe distance to prevent RF burns. The average off-diagonal noise correlation coefficient (Figure 7C) is comparable to that of a commercial head coil (16.5% and 18.9%). However, the overall decoupling performance was excellent. B1 mapping was also performed on a loading phantom as shown in Figure 7E–G. The B1 field was slightly influenced by the presence of the coil array but the lack of major artifacts indicated that the Q -spoiling circuitry was working properly.

In vivo images shown in Figure 8 revealed high signal near the surface of the brain.

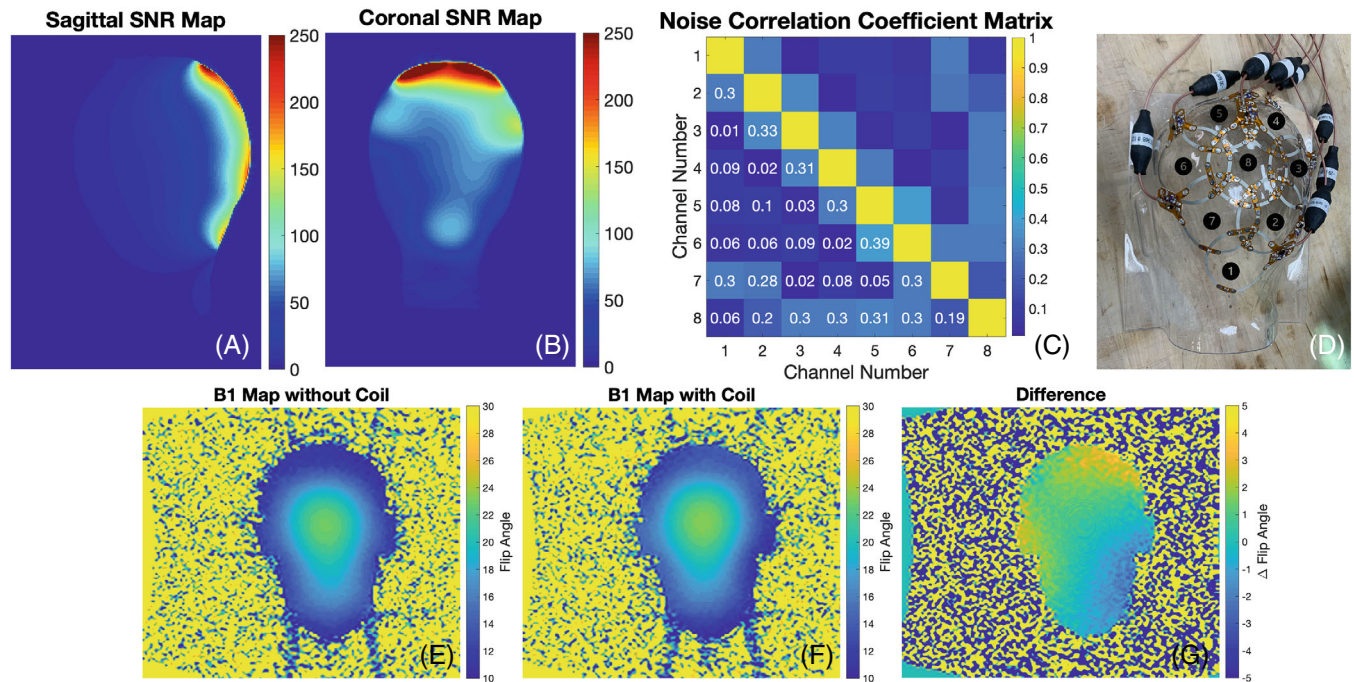


FIGURE 7 (A) Sagittal signal-to-noise ratio (SNR) map taken on a loading phantom using optimal coil combination and displayed in absolute units. (B) Coronal SNR map. (C) The noise correlation coefficient matrix. (D) Physical layout of the coil channels by coil number. (E) B1 map with a loading head-shaped phantom without the custom coil array. (F) B1 map with the 8 channel coil array on top. (G) Difference of the two showing the lack of major B1 variations.

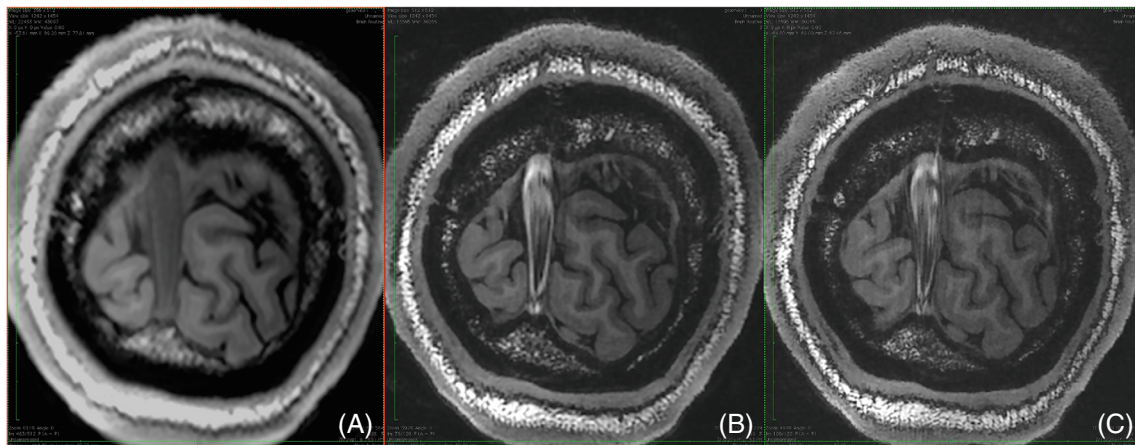


FIGURE 8 In vivo MR images of the visual cortex taken with our 8 channel coil. The images were acquired with a three-dimensional T1-weighted Bravo sequence with varying resolutions and no acceleration. The scan times were between 10 and 12 min. (A) Image taken with $1 \times 1 \times 1 \text{ mm}^3$ voxel size. (B) $0.5 \times 0.5 \times 0.67 \text{ mm}^3$. (C) $0.037 \times 0.37 \times 0.67 \text{ mm}^3$.

4 | DISCUSSION AND CONCLUSIONS

We present the first example of a receive coil for magnetic resonance imaging created with a combination of vacuum forming and electroless copper plating. With our method, it is possible to make coil arrays that place the receivers as close to the body as possible. This process may

enable the rapid development of a set of coils of different sizes. Though our example presented a coil for the visual cortex, it is possible to use our methods to design coils for other parts of the body. In addition, the ability to make bespoke arrays may be useful for applications that require motion restriction or reproducible subject placement, such as MR-guided radiation therapy or longitudinal fMRI studies.

Our process represents a major step toward additive manufacturing of MRI receive coils but there are many areas for improvement and future work. Though the mechanical simulation produces usable predistorted designs, we measured up to 1 cm of variation between the simulated plastic sheet and a 3D scanned physical sheet. This error was most apparent toward the edges of the head-shaped model since the plastic was stretched farther in those regions. The mechanical simulation could be improved by integrating more realistic plastic models as demonstrated in Reference 16.

We explored methods to verify the vacuum forming simulation by 3D scanning a grid printed onto a vacuum formed sheet. Due to the noise and quality of the scan, we were only able to reconstruct the central squares of the grid. In addition, our methods of filtering, edge detection, and construction of the connectivity grid could be improved. The reconstructed points overlaid on our simulated vacuum formed sheet are shown in Figure 2H. Despite having to ignore numerous grid points, the points that we were able to reconstruct cover the regions that were patterned by coil geometry.

The electrical simulation was performed with three channels on a surface that mimicked the curvature of the back of our head model. This could be improved by importing the full coil design (Figure 2F) from the mechanical simulation.

Construction of the coil with this method still requires manual work. The flex PCBs and other rigid components need to be soldered on with care to avoid melting the polycarbonate substrate. Each coil must still be tuned and matched with conventional methods. We did find that all of the coils required approximately the same series capacitance to tune them to the Larmor frequency. It was therefore much easier to finish the rest of the array once one coil was properly tuned and matched. This could improve the speed of manufacturing of MRI coils since the electrical traces can be repeatable patterned on a specific 3D substrate.

Though we focus on MRI coils, it would be possible to use these methods for any circuit. These techniques could expand electronic design beyond conventional, planar printed circuit boards.


FUNDING INFORMATION

The authors are fortunate to receive support from NIH Grants R01MH127104, U01EB029427, U01EB023829, and U01EB025162 as well as GE Healthcare.

DATA AVAILABILITY STATEMENT

The code for the graphical simulation used in this study is provided at github.com/mikgroup/Vacuum-Forming-Sim.

ORCID

Karthik Gopalan  <https://orcid.org/0000-0001-9836-1944>

REFERENCES

1. Roemer PB, Edelstein WA, Hayes CE, Souza SP, Mueller OM. The NMR phased array. *Magn Reson Med*. 1990;16:192-225.
2. Wiggins GC, Triantafyllou C, Potthast A, Reykowski A, Nitka M, Wald LL. 32-channel 3 tesla receive-only phased-array head coil with soccer-ball element geometry. *Magn Reson Med*. 2006;56:216-223.
3. Keil B, Alagappan V, Mareyam A, et al. Size-optimized 32-channel brain arrays for 3 T pediatric imaging. *Magn Reson Med*. 2011;66:1777-1787.
4. Zamarayeva AM, Gopalan K, Corea JR, et al. Custom, spray coated receive coils for magnetic resonance imaging. *Sci Rep*. 2021;11:1-9.
5. Corea JR, Flynn AM, Lechène B, et al. Screen-printed flexible MRI receive coils. *Nat Commun*. 2016;7:1-7.
6. Zhang B, Sodickson DK, Cloos MA. A high-impedance detector-array glove for magnetic resonance imaging of the hand. *Nature Biomed Eng*. 2018;2:570-577.
7. Vincent JM, Rispoli JV. Conductive thread-based stretchable and flexible radiofrequency coils for magnetic resonance imaging. *IEEE Trans Biomed Eng*. 2019;67:2187-2193.
8. Ernst M, Woop S. Embree: photo-realistic ray tracing kernels. White paper, Intel; 2011.
9. Zhang Y, Tong Y, Zhou K. Coloring 3D printed surfaces by thermoforming. *IEEE Trans Vis Comput Graph*. 2016;23:1924-1935.
10. Saboret L, Alliez P, Lévy B, Rouxel-Labbé M, Fabri A, Jain H. Triangulated surface mesh parameterization. CGAL User and Reference Manual. CGAL Editorial Board, 5.2.1 edition; 2021.
11. Liu L, Zhang L, Xu Y, Gotsman C, Gortler SJ. A local/global approach to mesh parameterization. *Computer Graphics Forum*. Vol 27. Blackwell Publishing Ltd; 2008:1495-1504.
12. Matijevic E, Poskanzer AM, Zuman P. Characterization of the stannous chloride/Palladium chloride catalysts for electroless plating. *Plat Surf Finish*. 1975;62:958-965.
13. Kao CY, Chou KS. Electroless copper plating onto printed lines of nanosized silver seeds. *Electrochem Solid-State Lett*. 2007;10:D32.
14. Veleva R. Role of potassium ferrocyanide in electroless copper baths. *Surf Coat Technol*. 1989;29:87-93.
15. Kellman P, McVeigh ER. Image reconstruction in SNR units: a general method for SNR measurement. *Magn Reson Med*. 2005;54:1439-1447.
16. Schüller C, Panozzo D, Grundhöfer A, Zimmer H, Sorkine E, Sorkine-Hornung O. Computational thermoforming. *ACM Trans Graph*. 2016;35:1-9.

SUPPORTING INFORMATION

Additional supporting information may be found in the online version of the article at the publisher's website.

Figure S1. Electroless plating with a smaller sample. (A) Our electroless copper plating setup including a polypropylene tank, circulation pump, filter bag, and nitrogen line. (B) A small vacuum formed sample after copper plating to showcase the capabilities of our method.

(C) Demonstration of soldering a resistor to the plated copper traces

Figure S2. (A) The circuit diagram of a single channel with Q-spoiling and matching circuitry. The coil is connected to a 16-channel preamplifier box and measured with a network analyzer. (B) The S_{11} measurement of a tuned and matched coil connected directly to the network analyzer. (C) Measurements of the coil when connected to the preamplifier. The red trace shows the detuned state when the PIN diode is biased.

Figure S3 (A) Pair of printed circuit boards used to form a single trap. (B) The two boards soldered together to make a winding guide. (C) The coaxial cable wound and attached to the board. (D) The placement of the clear three-dimensional printed shield before adding copper tape. (E) Trap attached to measurement setup. (F) S_{21} of a single trap

Figure S4. Copper plating experiments on small strips of polycarbonate. The strips on top from left to right were left bare, hand sanded with 120 grit sand paper, hand sanded with 320 grit sand paper, and sandblasted with 100 grit white fused aluminum oxide blasting media. All strips were cleaned, catalyzed, and copper plated. Red arrows reveal defects in the copper plating. This indicates that a surface treatment is necessary for copper adhesion and sandblasting produces the most uniform results.

How to cite this article: Gopalan K, Maravilla J, Mendelsohn J, Arias AC, Lustig M. Vacuum formed coils for MRI. *Magn Reson Med.* 2023;89:1684-1696. doi: 10.1002/mrm.29546